Neurosci Bull August 1, 2012, 28(4): 321–332. http://www.neurosci.cn
DOI: 10.1007/s12264-012-1249-z

·Review·

Ultrastructural analysis of neuronal synapses using state-of-the-art nano-imaging techniques

Changlu Tao[1,*], Chenglong Xia[1,*], Xiaobing Chen[2], Z. Hong Zhou[1,3], Guoqiang Bi[1]

[1]*Center for Integrative Imaging, Hefei National Laboratory for Physical Sciences at the Microscale & School of Life Sciences, University of Science and Technology of China, Hefei 230027, China*
[2]*Laboratory of Neurobiology, National Institute of Neurological Disorders and Stroke, National Institutes of Health, Bethesda, 20892, USA*
[3]*Department of Microbiology, Immunology & Molecular Genetics, University of California, Los Angeles, Los Angeles, CA 90095-7364, USA*

Abstract: Neuronal synapses are functional nodes in neural circuits. Their organization and activity define an individual's level of intelligence, emotional state and mental health. Changes in the structure and efficacy of synapses are the biological basis of learning and memory. However, investigation of the molecular architecture of synapses has been impeded by the lack of efficient techniques with sufficient resolution. Recent developments in state-of-the-art nano-imaging techniques have opened up a new window for dissecting the molecular organization of neuronal synapses with unprecedented resolution. Here, we review recent technological advances in nano-imaging techniques as well as their applications to the study of synapses, emphasizing super-resolution light microscopy and 3-dimensional electron tomography.

Keywords: synaptic architecture; nano-imaging; super-resolution imaging; STED microscopy; STORM; PALM; cryoET

1 Introduction: a brief history of synapse imaging

Since the beginning of modern neuroscience when Cajal's vivid drawings revealed neurons and their connections in the nervous system, synapses have been regarded as the key nodes for neuronal communication[1,2]. It is now believed that structural and functional changes in these nodes form the cellular substrate of learning and memory, as well as various neurological and psychiatric disorders[3,4].

Microscopic imaging techniques have always played prominent roles in our understanding of neurons and synapses. Historically, light microscopy (LM) with Golgi staining allowed morphological analysis as well as functional interpretation of neurons and neuronal circuits[2,5]. Based on anatomical observations under LM, Cajal reasoned more than a century ago that there are "more or less intimate contacts" formed between the nerve arborizations (i.e. axons) and the body and protoplasmic processes (i.e. dendrites) that serve for transmitting signals[2,5]. Such a "contact" indeed turned out to be a specialized communication device, later termed "synapse" by Foster and Sherrington[6,7]. The key elements of Cajal's successes, besides his personal genius, were the improved LM of his time and the unique Golgi staining method where silver salt labeled only a

*These authors contributed equally to this work.
Corresponding author: Guoqiang Bi
Tel & Fax: +86-551-3602466
E-mail: gqbi@ustc.edu.cn
Article ID: 1673-7067(2012)04-0321-12
Received date: 2012-06-14; Accepted date: 2012-06-26

small fraction of the neurons but outlined the elaborate processes of single neurons in their entirety. The silver-impregnated neurons, seen through chromatically corrected optics and Cajal' artistic eyes, provided the first view of the organization of the nervous system[1,8].

The direct demonstration of synapses and their fine structural details awaited the emergence of electron microscopy (EM) in the 1950s. Taking advantage of the exquisite spatial resolution of transmission electron microscopy (TEM), Palay and Gray gave the first systemic description of the fine details of the synapse[9-12]: a presynaptic terminal filled with synaptic vesicles, a postsynaptic terminal lined with an electron dense thickening called the postsynaptic density (PSD), and the gap separating the two terminals, the synaptic cleft. In 1973, Heuser and Reese reported evidence of fusion and recycling of synaptic vesicles in the neuromuscular junction under various stimulus conditions, thus revealing the nature of synaptic transmission[13]. Since the 1980s, serial section TEM (ssTEM) involving reconstruction of serial sections of neuronal processes and synapses with high spatial resolution, has enabled 3-dimensional (3D) imaging of entire dendritic arbors, synapses, as well as detailed organelles at the synapses such as synaptic vesicles and PSDs[14].

In the past decades, molecular and biochemical analyses contributed tremendously to our understanding of the synapse by identifying a growing set of molecular components and signaling pathways[15]. Meanwhile, modern neuroscience has flourished with fluorescence microscopy. The multitude of labeling methods, including targeting specific proteins with different fluorophore-tagged antibodies and expressing fluorescent fusion proteins of various colors, has allowed specific and precise assessment of gene expression and protein localization in both fixed and live cells and synapses[16,17]. However, our knowledge of the architecture of synapses and the molecular organization of synaptic proteins has been limited to coarse qualitative descriptions[18]. The small size of the synapse is the major technological bottleneck. Conventional LM, including fluorescent microscopy, limited by the ~200 nm resolution set by diffraction[19], can determine the presence of certain synaptic proteins in a synapse, but not their spatial relationships. In conventional EM that is of much higher resolution, biological samples usually undergo sample preparation procedures, including chemical fixation, dehydration, embedding, and heavy metal salt staining, which often compromise the native ultrastructure and produce artifacts[20].

In recent years, the rapid development of new biophysical methods and powerful image-processing algorithms has opened a new page in nano-imaging. In particular, super-resolution fluorescence LM, including stimulated emission depletion (STED) microscopy[21], reversible saturable optically linear fluorescence transitions (RESOLFT)[22], saturated structured-illumination microscopy (SSIM)[23], stochastic optical reconstruction microscopy (STORM)[24], photo-activated localization microscopy (PALM)[25], and fluorescence photo-activation localization microscopy (FPALM)[26], has broken the diffraction limit and the resolution can be tens of nanometers. Meanwhile, electron tomography (ET)[27] combined with cryo-sample preparation techniques[20] has provided ultrastructural 3D information at nanometer resolution of biological targets in their near-native state. In this article, we review recent technological advances in both super-resolution fluorescence microscopy and 3D ET, highlighting their current and potential applications in the study of synaptic structure and function.

2 Super-resolution fluorescence microscopy

From the naked eye to LM, to EM, the history of microscopic biology is accompanied by resolution improvement. Conventional fluorescence LM is the most widely-used imaging technique in cellular studies because it can achieve high sensitivity, high contrast, multi-color labeling and live imaging[28]. Nevertheless, its resolution is limited by the diffraction property of light, such that the image of a single point light source becomes a disk called the Airy disk, or more generally the point-spread function. The resolution limit is often described by the Abbe limit, $d = \lambda/2\mathrm{NA}$ (where d is the smallest distance between two particles that can be resolved, λ is the wavelength of light, and NA is the numerical aperture of the objective lens)[19].

For visible light (λ ~500 nm) and a good microscope lens (NA ~1.2), the resolution limit is ~200 nm. With an electron beam (usually λ_e<<1 nm), EM can easily achieve nanometer resolution. However, compared to LM, conventional EM is limited to fixed samples and a lack of specific labeling of different target molecules at high-density with various colors. Therefore, it is desirable to improve the resolution of fluorescence LM.

Super-resolution fluorescence microscopy techniques can be divided into two types according to the principles they use to break the diffraction limit. In the first type, including STED microscopy and its generalized form of RESOLFT microscopy developed by Hell and colleagues[21,22], and SSIM developed by Gustafsson and colleagues[23], nonlinear optical effects are used to sharpen the point-spread function of the microscope system. The other type, including STORM developed by Zhuang and colleagues[24], PALM developed by Betzig and colleagues[25] and fPALM developed by Mason and colleagues[26], is based on the computed localization of individual fluorescent molecules from their diffraction limited non-overlapping images.

The optical configuration of STED microscopy is similar to that of confocal laser scanning microscopy, but with an extra donut-shaped STED light pattern that causes stimulated fluorescence emission of illuminated fluorophores[21,22]. When the STED light intensity is strong, the stimulated emission brings all excited fluorophores down to the ground state (stimulated emission depletion)[21]. Thus, only the center of the donut ring, where STED light intensity is low enough, can emit fluorescence spontaneously, usually at wavelengths slightly different from the STED light (Fig. 1A, B). Theoretically, STED microscopy can attain unlimited resolution by using an infinitely intense depletion light source. However, fluorescence bleaching as well as aberrations in the optics and scattering from the sample limit the resolution of STED microscopy to tens of nanometers[29]. When combined with 4Pi microscopy[30], isoSTED[31] can achieve ~30 nm resolution in all three axes[32]. The newer RESOLFT microscopy based on saturated transitions was developed to alleviate fluorophore bleaching and sample damage in STED microscopy[33].

One highlight of STED microscopy is its ability to achieve imaging depth. Combined with two-photon excita-

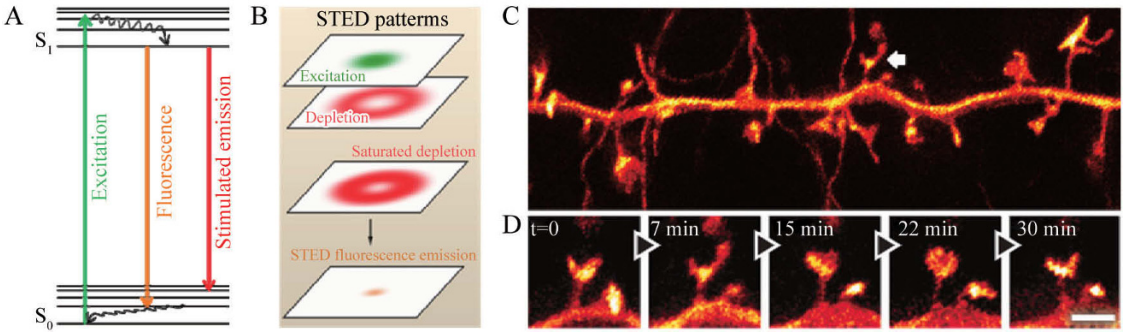

Fig. 1. Stimulated emission depletion (STED) microscopy. A: Energy level diagram illustrating the principle of STED: when the fluorophore absorbs excitation light and transitions to the excited state, it can spontaneously transition back to the ground state while emitting lower-energy fluorescence light. However, in the presence of a stimulation light, stimulated emission can occur and deplete the fluorophore from the excited state, thus reducing the amount of spontaneous fluorescence emission. B: In STED microscopy, the excitation laser spot (green, top layer) overlaps with a concentric donut-shaped depletion laser light pattern (red, second layer) generated by a spatial light modulator. The depletion light brings all excited-state fluorophores in the "donut" to the ground state and prevents fluorescence emission except for the center spot (orange, bottom layer). Depending on the intensity of the depletion light, the size of the center spot that can emit fluorescence can be substantially smaller than the original excitation spot, thus achieving high image resolution beyond the optical diffraction limit. C: A dendritic process within the molecular layer of the somatosensory cortex of a Thy1-EYFP mouse, imaged by an upright scanning STED fluorescence microscope. D: Zoom-in view of a dendritic spine (white arrow in C), showing the temporal dynamics of spine morphology (Scale bar, 1 μm). (B adapted from Huang *et al.*, 2010[29] with permission; C and D adapted from Berning *et al.*, 2012[36] with permission).

tion, STED was used to image dendritic spines ~100 μm below the surface of brain slices[34]. By using aberration-reducing optics, STED microscopy achieved a resolution of 60–80 nm, 120 μm deep inside scattering biological tissue[35]. More recently, STED microscopy has been used to image spine dynamics in the cerebral cortex of a living mouse (Fig. 1C, D)[36]. In other applications, two-color STED images of *Drosophila* Rab3-interacting molecule-binding protein (DRBP) and Bruchpilot at *Drosophila* neuromuscular junctions demonstrated the relative spatial locations and shapes of these two proteins, and revealed that DRBP is essential for neurotransmitter release[37]. 3D dual-color isoSTED nanoscopy of Syt1 and RRetP in presynaptic boutons of cultured hippocampal neurons suggested preferential recruitment of a surface pool of synaptic vesicle proteins[38]. STED has also been used to visualize the reserve pool of synaptic vesicles[39].

The principle of STORM/PALM is based on high accuracy in locating single molecules that emit strong fluorescence. Using switchable fluorescence probes that can be activated one (or a few) at a time, it is possible to image individual probe molecules without spatial overlap, thus avoiding the diffraction limit[40]. By calculating the locations of activated molecules iteratively, the spatial distribution of a large number of probes can be obtained to reconstruct a super-resolution image of the probed structure (Fig. 2A). With dual-objective STORM, better than 10-nm lateral resolution and 20-nm axial resolution have been obtained to resolve the distribution of actin filaments in various cell lines[41]. Access to various photoactivatable proteins and a large number of photoswitchable fluorophore configurations enables STORM/PALM to easily achieve multicolor imaging[42-44].

Because the detection of single molecule fluorescence requires a very low background, STORM/PALM is currently limited to thin samples and is hard to apply to tis-

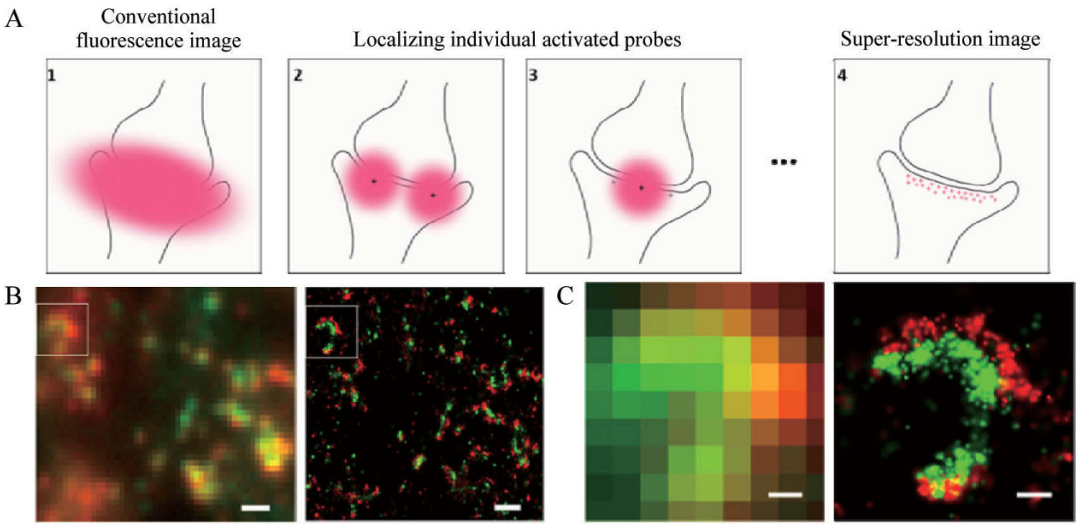

Fig. 2. Super-resolution imaging of synaptic scaffolding proteins by stochastic optical reconstruction microscopy (STORM). A: Schematic diagram showing the principle of STORM imaging. In conventional fluorescence microscopy, the image of a putative postsynaptic protein is blurry due to optical diffraction (A1). In STORM imaging, most fluorescent probes labeling individual protein molecules are switched to a dark state; only a sparse subset of molecules is activated and optically resolved at one time. The location of each molecule is then computed as the center of the corresponding Airy disk (A2, A3). After many iterations of this process, a super-resolution image of the target protein can be reconstructed from thousands of frames of qualified localization data (A4). B: Optical localization of presynaptic protein Bassoon (red) and postsynaptic protein Homer1 (green) in the mouse main olfactory bulb glomeruli by immunohistochemistry using Cy3-Alexa647- and Alexa405-Alexa647-conjugated antibodies. Left: Conventional fluorescence image; right: STORM image (Scale bars, 1 μm). C: Zoom-in view of a small area in B (Scale bars, 200 nm). (B and C adapted from Dani *et al*., 2009[47] with permission).

sue slices or live animals. When imaging live samples, STORM is relatively slow due to the necessity of accumulating a large number of single-molecule images to obtain a super-resolution reconstruction. Compared to STED, STORM is slower when imaging a small region[40]. For larger fields of view, however, 3D STORM based on wide-field imaging can be faster than STED that is based on point laser scanning. In a live neuron imaging study with a $2.5 \times 1.8\ \mu m^2$ field of view, STED imaging achieved a video-rate of 28 frames per second (fps) at 62 nm spatial resolution[45]. Meanwhile, 3D STORM imaging of live cells in a field of view of up to $30 \times 15\ \mu m^2$ achieved a rate of 0.5–1 fps with ~30 nm lateral and ~50 nm axial resolution[46].

STORM imaging has been used to analyze the organization of ten synaptic proteins in the presynaptic active zone and the PSD (Fig. 2B, C)[47]: Bassoon, Homer1, Shank1, Piccolo, PSD95, GluR1, NR2B, CaMK II, RIM1 and $GABA_BR1$. The numbers and relative locations of these molecules were characterized by quantitative analysis. Even the orientation of Homer1 was determined based on the location of its N- and C-terminus-specific antibodies. In addition, STORM imaging can clearly reveal changes in the number of NR2B relative to GluR1 molecules in a synapse following light stimulation[47].

Similar to STORM/PALM that take advantages of single-molecule fluorescence imaging, single-particle tracking (SPT) has been used to monitor the motion of individual protein molecules in living cells. With this approach, it was found that the polymerization rate of PA-GFP-labeled actin molecules in the postsynaptic compartment differs from that in the nearby endocytic zone[48]. Analysis of the mobility of individual AMPA receptors (AMPARs) with SPT revealed that the ratio of mobile to immobile AMPARs changes with glutamate application or blockade of inhibitory transmission to favor excitatory synaptic activity[49]. In addition, results from SPT of AMPARs within or near the PSD suggested that the lateral diffusion of AMPARs might permit the desensitized receptors to be rapidly exchanged for functional ones, thus pointing to a postsynaptic regulatory mechanism of synaptic transmission[50]. On the other hand, a more recent study using photobleaching and fluorescence correlation analysis suggested that the postsynaptic scaffold is largely responsible for clustering AMPARs[51].

3 Cellular ET

The latest super-resolution techniques of fluorescence imaging have greatly enhanced our ability to probe the molecular organization and dynamics in cells and synapses. However, the flip-side of the specificity of fluorescence imaging is that unlabeled proteins, presumably constituting the majority of any cellular compartment under investigation, simply cannot be seen. Besides the few labeled "trees", it is often desirable to also see the unlabeled "forest" to understand the complex architecture of macromolecules and cellular organelles inside a synapse. EM, especially the newly improved 3D ET[27], is a powerful tool for this purpose.

Different from fluorescent microscopy, where the contrast arises from the specific fluorescence excitation and emission properties of different fluorophores, the main contrast in EM comes from electron scattering, which is uniformly low for molecules in biological specimens, such as a cell. Therefore, heavy metal elements which scatter electrons strongly and often bind to proteins are added to stain biological samples. Alternatively, weak scattering of incoming electron beams by the specimen modulates their phases. By defocusing the electron microscope or using a phase plate, the phase differences can be converted to amplitude differences in the image plane, generating "phase-contrast" images of biological molecules and cellular organelles without staining.

ET is based on the 3D reconstruction theory of EM proposed by Derosier and Klug in the 1960s[52]. The principle is that a 3D ultrastructure of the sample can be obtained at nanometer resolution by back-projecting a set of tilt series of high-resolution 2D TEM projections of the target into a 3D map[27] (Fig. 3). Another key component for successful high-resolution ET is cryo-fixation that better preserves the native ultrastructure during specimen preparation[20,27]. In cryo-fixation, biological samples in their native buffer environment are rapidly cooled to about

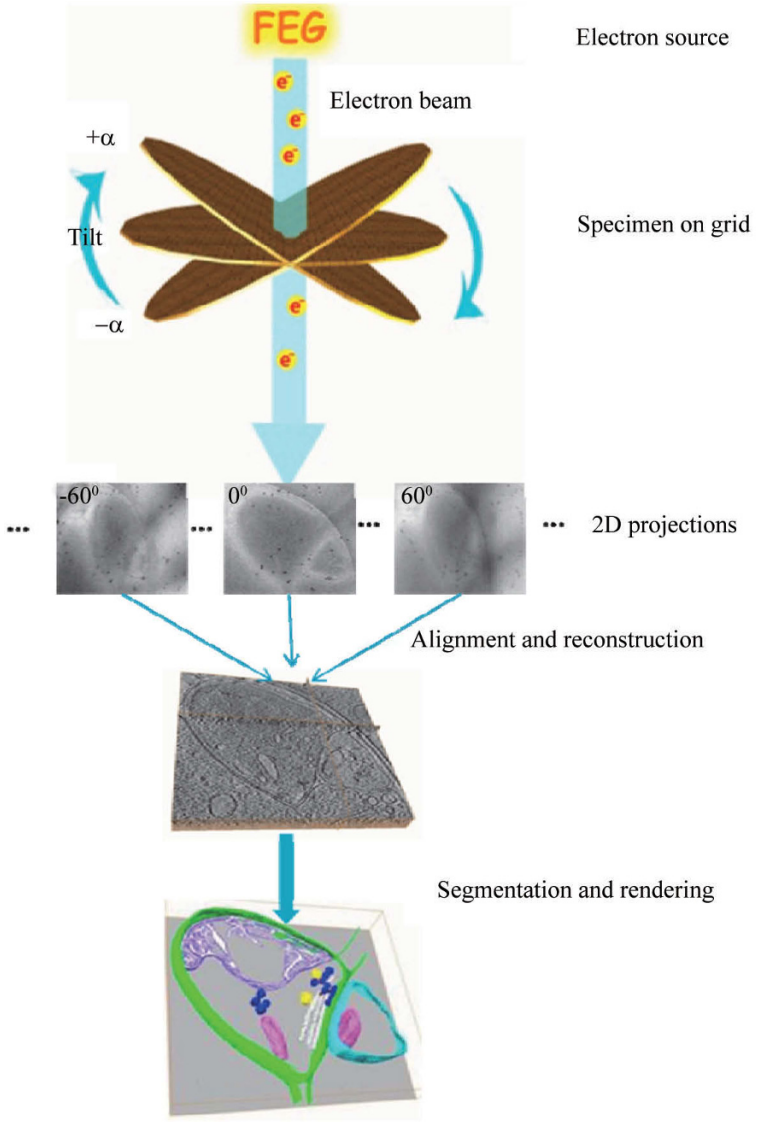

Fig. 3. Flowchart of electron tomography. The specimen is tilted incrementally along an axis perpendicular to the electron beam (preferentially supplied by a field emission gun). Tilt increments are typically 1–2° and the tilt range is approximately ± 60–70°. 2D projections of the same specimen area are imaged one at a time. After precise mutual alignment, these projection images are synthesized into a 3D density map by the 'weighted back projection' procedure. A more visually explicit 3D model of specific targets in the density map is often created by segmentation and rendering in order to facilitate measurement and interpretation.

−180ºC or below in cryogens (e.g. liquid ethane) within milliseconds. In this process, water molecules in the sample are fixed in a non-crystalline vitreous state. In contrast to chemical fixation, cryo-fixation is fast, does not introduce changes in the state of the specimen, and is capable of preserving biological ultrastructure at the atomic scale[53-55]. Common cryo-fixation methodology has two approaches, plunge-freezing for thin samples (up to 20 μm thick) and high-pressure freezing for bulk samples (as thick as 200 μm)[20,56]. However, because of the deterioration of imaging quality caused by inelastic scattering and multiple scattering that is more significant in thicker samples[27], the effective thickness of organic samples for high-resolution ET is limited to ~500 nm[57]. Thicker samples must be sectioned

by cryo-ultramicrotomy[58], or sectioned at room temperature after freeze-substitution and embedding[59,60].

ET has now been widely used to solve, at nanometer resolution, the 3D structures of dynamic or pleomorphic objects, such as macromolecular complexes[61], viruses[62], bacteria[63], cellular organelles[64], whole cells[65], and tissue slices[66], preserved in a close-to-life state[27]. With rapid cryo-fixation, ET can be used to take snapshots of dynamic processes in biological systems[67], achieving a resolution of 1–6 nm. In practice, ET can be used in combination with LM, X-ray crystallography and other structural biology approaches[68,69] to provide structural insights into large molecular complexes in cells and to facilitate the analysis of structure-function relationships.

The common length scale studied under high-magnification ET is usually a couple of micrometers, ideally matching the size of a synapse. Because of the depth limitation of electron penetration, four types of synaptic preparations have been used in ET studies: synaptosomes[65,66,70], monolayer primary neuronal cultures[65,69,71], cryo-sections of brain tissues after high-pressure freezing[65], and freeze-substitution of neuronal cultures or brain tissues followed by embedding and regular sectioning[59,60]. With these approaches, fascinating details of the synapse have begun to be uncovered, as described below.

3.1 Organization of synaptic vesicles in the presynaptic cytomatrix There are hundreds of neurotransmitter-filled synaptic vesicles in a presynaptic terminal. These vesicles are thought to be embedded in a filamentous network called the presynaptic cytomatrix, which plays essential roles in mediating vesicle trafficking. However, the precise organization and regulation of synaptic vesicles are still not understood. Studies using conventional EM suggested that vesicles are linked together by short connectors and to longer actin filaments through other short connectors[72,73]. Recent cryoET analysis of frozen-hydrated synaptosomes and hippocampal slices[65,66] showed that most synaptic vesicles are linked by short (<40 nm) filaments (connectors). However, longer actin filaments are rarely seen in the presynaptic cytomatrix. Our observations on frozen-hydrated neuronal cultures (Fig. 4) are consistent with the latter. These results argue against a major role of actin filaments in vesicle clustering under native conditions. At the active zone, vesicles are linked to the presynaptic membrane by tethers (Fig. 4B), consistent with the results from frozen-hydrated synaptosomes and hippocampal slices[65,66]. Although their molecular identities are still unknown, these connectors and tethers are likely to play important roles in vesicle recycling as well as docking and fusion events.

3.2 Molecular organization of the synaptic cleft In a chemical synapse, the synaptic cleft is a 20–25-nm gap between the presynaptic and postsynaptic cells. Several families of cell adhesion molecules are located in the cleft, and are thought to regulate synaptic development, synaptic plasticity and signal transduction between pre- and postsynaptic compartments[74,75]. CryoEM analysis of synapses in vitreous sections of rat hippocampal slices showed that the material in the synaptic cleft is electron-dense, and the trans-cleft complexes are organized with a periodicity of 8.2 nm[58]. CryoET analysis of frozen-hydrated synaptosomes showed that the density of the material in the synaptic cleft is the highest in the central region of the cleft[70]. A 3-nm tomographic section from frozen-hydrated neuronal culture (21 days *in vitro*) from our data confirmed the above observations (Fig. 4).

3.3 Organization of the core structure of the PSD The PSD was first recognized by EM as a band of electron-dense material anchored to the cytoplasmic side of the postsynaptic membrane, about 30 nm thick and 300 nm long[9,12]. It is now known to consist of complex signaling machinery containing receptors, signaling molecules, and scaffolding complexes[76]. A dense network of vertical and horizontal filaments was revealed in tomograms of hydrated-frozen synaptosomes and neuronal cultures[65,66,69]. In freeze-substituted sections of rat hippocampal cultures, the organization of the PSD of the glutamatergic synapse has been further delineated by ET, with putative NMDA- and AMPA-type glutamate receptors identified (Fig. 5)[59,60]. Interestingly, NMDA receptors were found to be located in the central part of the PSD and were contacted by one or two vertical filaments, whereas AMPARs were distributed around the periphery of the PSD, consistent with many

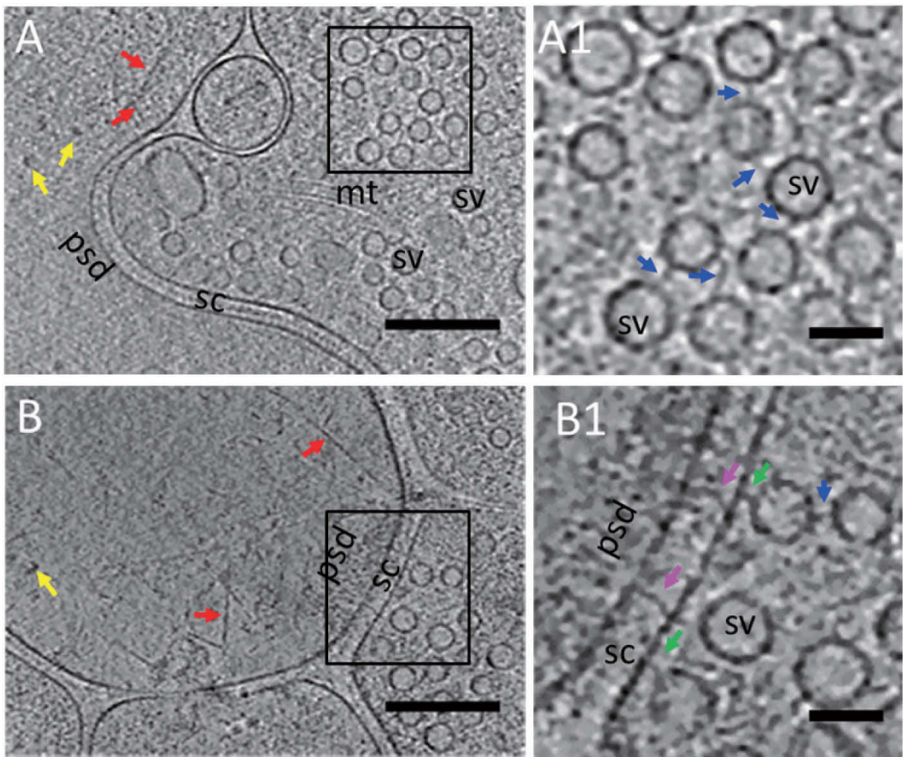

Fig. 4. Ultrastructural dissection of synapses by cryo electron tomography. A: A 3-nm tomographic section through an identified synapse in hippocampal culture frozen-hydrated at 21 days *in vitro* (DIV). Arrows indicate putative actin filaments (red) and ribosomes (yellow). Other identifiable structures include synaptic vesicles (sv), microtubules (mt), synaptic cleft (sc), and postsynaptic density (psd). A zoom-in view of the boxed region is shown in A1. Putative connectors (blue arrows) can be seen to link vesicles together. B: A 3-nm tomographic section through another synapse (16 DIV). The boxed region is magnified in B1, where tethers linking vesicles to the presynaptic membrane (green arrows) and a connector (blue arrow) linking another vesicle to one of the docked vesicles can be identified. Also seen are transcleft complexes (pink arrows). Scale bars for A and B, 200 nm; A1 and B1, 50 nm.

observations from immuno-EM[77,78]. Two types of horizontal filaments were identified: the shorter type is 4–5 nm in diameter and about 20 nm long, and the longer type is 5–6 nm in diameter and 30–35 nm long. The shorter filaments link both NMDA receptors and AMPARs, whereas the longer horizontal filaments link adjacent NMDA receptors. This organization indicates the instability of AMPARs relative to NMDA receptors, consistent with their roles in the expression of synaptic plasticity.

4 Where the future lies…

After over a hundred years of investigation, we understand a great deal about the complexity of the synapse, though often as a tiny black box[3]. Now, with the emergence of nano-imaging techniques that promise to open the black box, the organization and operation of the delicate nano-machinery inside can be revealed. Our understanding of this key communication device is poised to enter a new era. Surely, many obstacles still exist: STORM imaging is relatively slow and limited to thin specimens; STED microscopy is limited by fluorophore selection and often suffers from photobleaching; and cryoET is low-throughput, low-contrast, and cannot directly identify protein targets. Still higher resolution is required. Last but not least, there is no universal computational framework that can put the myriad of data together.

Nevertheless, the technological front of nano-imaging is moving (and accelerating) so rapidly that it is time for synaptic biologists and biophysicists to seriously consider using these new approaches in their research and to iden-

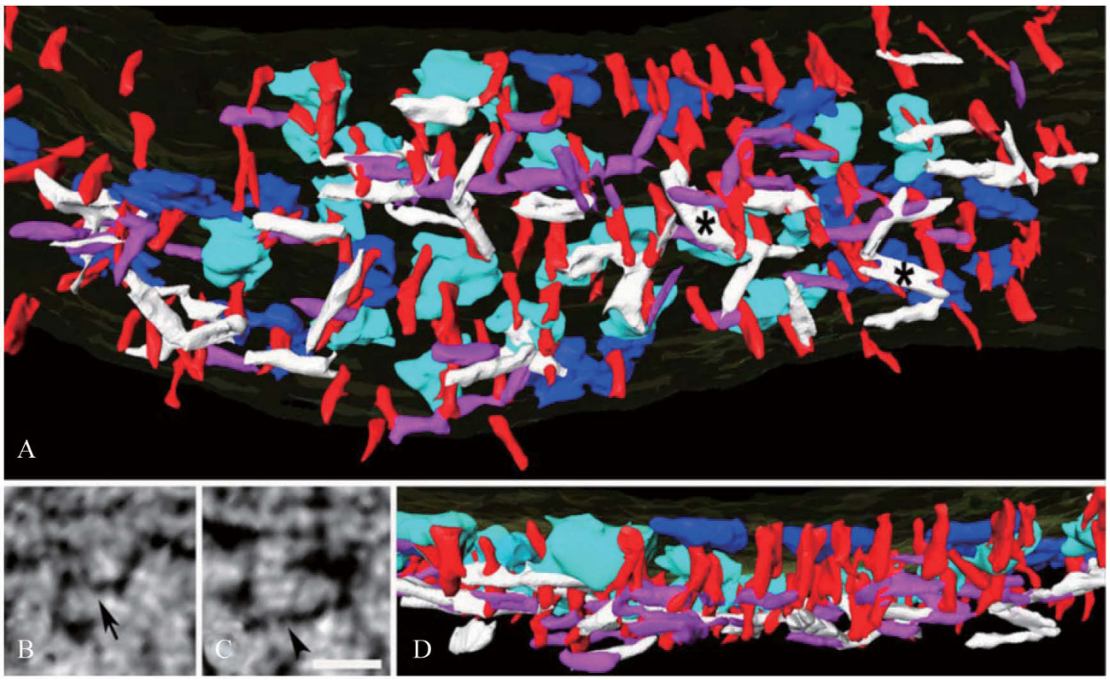

Fig. 5. Postsynaptic organization of a glutamatergic synapse. A tomographically imaged 200-nm section through a dendritic spine of a cultured hippocampal neuron prepared by freeze-substitution. Fine structural details are segmented and rendered from the tomogram. A: Cytoplasmic surface view of the 3D architectural network at the core of the PSD, showing cytoplasmic domains of AMPAR-type structures (blue) and NMDAR-type structures (cyan), vertical filaments (red), and two types of horizontal filaments (purple: the shorter type, 4–5 nm in diameter and ~20 nm long; white: the longer type, 5–6 nm in diameter and 30–35 nm long). Asterisks indicate sheet-like structures. B and C: Two tomographic slices that contain shorter (B, arrow) and longer (C, arrowhead) types of horizontal filaments. Scale bar, 20 nm. D: Cross-sectional view of the PSD. (From Chen *et al*., 2008[59] with permission).

tify, and perhaps help overcome new technical bottlenecks in the meantime. Indeed, brighter fluorescent dyes, faster cameras and new optical methods are being developed to further improve fluorescence nanoscopy[29,79]. New EM hardware such as Cs-corrector[80], phase-plate[81,82] and direct detection device[83], together with new software like CTF correction[84], template-match[85] and sub-average[61], promises to improve the contrast and resolution of cryo-tomograms. Furthermore, along the line of correlative microscopy, and by taking advantages of LM-EM protein tags such as miniSOG[86], combining super-resolution fluorescence LM with cryoET would likely bring about major advances in synaptic neuroscience and biomedical research in general. With these advances, a future is foreseeable where we may unravel the mysteries of the synapse, and in a bottom-up fashion, neural circuits and the brain.

Acknowledgements: We thank Peijun Zhang for technical advice on cryoET, Yuntao Liu for help with figure drawing, and Cheng Xu, Nico Wagner, Xiaowei Zhuang and Pakming Lau for helpful discussions. This review was partly supported by grants from the National Natural Science Foundation of China (30725017 and 30928003) and MOST (2009CB941300).

References:

[1] Cajal SR. The Structure and Connexions of Neurons. Nobel Lecture, 1906. URL: http://nobelprize.org/medicine/laureates/1906/cajal-lecture.html.

[2] DeFelipe J. From the connectome to the synaptome: An epic love story. Science 2010, 330: 1198–1201.

[3] Mayford M, Siegelbaum SA, Kandel ER. Synapses and memory storage. Cold Spring Harb Perspect Biol 2012, 4. doi: 10.1101/cshperspect. a005751.

[4] Goto Y, Yang CR, Otani S. Functional and dysfunctional synaptic plasticity in prefrontal cortex: roles in psychiatric disorders. Biol Psychiatry 2010, 67: 199–207.

[5] Llinas RR. The contribution of Santiago Ramon y Cajal to functional neuroscience. Nat Rev Neurosci 2003, 4: 77–80.

[6] Sherrington CS. The Integrative Action of the Nervous System. New York: Charles Scribner's Sons, 1906.

[7] Foster. M, Sherrington CS. A Textbook of Physiology. 7th ed. London: MacMillan & Co Ltd, 1897.

[8] Lopez-Munoz F, Boya J, Alamo C. Neuron theory, the cornerstone of neuroscience, on the centenary of the Nobel Prize award to Santiago Ramon y Cajal. Brain Res Bull 2006, 70: 391–405.

[9] Palay SL. Synapses in the central nervous system. J Biophys Biochem Cytol 1956, 2: 193–202.

[10] Palay SL. The morphology of synapses of the central nervous system. Exp Cell Res 1958, 14: 275–293.

[11] Gray EG. Axo-somatic and axo-dendritic synapses of the cerebral cortex: an electron microscope study. J Anat 1959, 93: 420–433.

[12] Gray EG. Electron microscopy of synaptic contacts on dendrite spines of the cerebral cortex. Nature 1959, 183: 1592–1593.

[13] Heuser JE, Reese TS. Evidence for recycling of synaptic vesicle membrane during transmitter release at frog neuromuscular junction. J Cell Biol 1973, 57: 315–344.

[14] Harris KM, Weinberg RJ. Ultrastructure of synapses in the mammalian brain. Cold Spring Harb Perspect Biol 2012, 4. doi: 10.1101/cshperspect.a005587.

[15] Sheng M, Hoogenraad CC. The postsynaptic architecture of excitatory synapses: a more quantitative view. Annu Rev Biochem 2007, 76: 823–847.

[16] Wilt BA, Burns LD, Ho ETW, Ghosh KK, Mukamel EA, Schnitzer MJ. Advances in light microscopy for neuroscience. Annu Rev Neurosci 2009, 32: 435–506.

[17] Giepmans BN, Adams SR, Ellisman MH, Tsien RY. The fluorescent toolbox for assessing protein location and function. Science 2006, 312: 217–224.

[18] Bayes A, Grant SGN. Neuroproteomics: understanding the molecular organization and complexity of the brain. Nat Rev Neurosci 2009, 10: 635–646.

[19] Hell SW. Microscopy and its focal switch. Nat Methods 2009, 6: 24–32.

[20] Hurbain I, Sachse M. The future is cold: cryo-preparation methods for transmission electron microscopy of cells. Biol Cell 2011, 103: 405–420.

[21] Hell SW, Wichmann J. Breaking the diffraction resolution limit by stimulated emission:stimulated-emission-depletion fluorescence microscopy. Opt Lett 1994, 19: 780–782.

[22] Hell SW. Far-field optical nanoscopy. Science 2007, 316: 1153–1158.

[23] Gustafsson MG. Nonlinear structured-illumination microscopy: wide-field fluorescence imaging with theoretically unlimited resolution. Proc Natl Acad Sci U S A 2005, 102: 13081–13086.

[24] Rust MJ, Bates M, Zhuang X. Sub-diffraction-limit imaging by stochastic optical reconstruction microscopy (STORM). Nat Methods 2006, 3: 793–795.

[25] Betzig E, Patterson GH, Sougrat R, Lindwasser OW, Olenych S, Bonifacino JS, *et al.* Imaging intracellular fluorescent proteins at nanometer resolution. Science 2006, 313: 1642–1645.

[26] Hess ST, Girirajan TP, Mason MD. Ultra-high resolution imaging by fluorescence photoactivation localization microscopy. Biophys J 2006, 91: 4258–4272.

[27] Lucic V, Forster F, Baumeister W. Structural studies by electron tomography: from cells to molecules. Annu Rev Biochem 2005, 74: 833–865.

[28] Dani A, Huang B. New resolving power for light microscopy: applications to neurobiology. Curr Opin Neurobiol 2010, 20: 648–652.

[29] Huang B, Babcock H, Zhuang XW. Breaking the diffraction barrier: super-resolution imaging of cells. Cell 2010, 143: 1047–1058.

[30] Dyba M, Hell SW. Focal spots of size λ/23 open up far-field florescence microscopy at 33 nm axial resolution. Phys Rev Lett 2002, 88: 163901.

[31] Schmidt R, Wurm CA, Jakobs S, Engelhardt J, Egner A, Hell SW. Spherical nanosized focal spot unravels the interior of cells. Nat Methods 2008, 5: 539–544.

[32] Schmidt R, Wurm CA, Punge A, Egner A, Jakobs S, Hell SW. Mitochondrial cristae revealed with focused light. Nano Lett 2009, 9: 2508–2510.

[33] Hofmann M, Eggeling C, Jakobs S, Hell SW. Breaking the diffraction barrier in fluorescence microscopy at low light intensities by using reversibly photoswitchable proteins. Proc Natl Acad Sci U S A 2005, 102: 17565–17569.

[34] Ding JB, Takasaki KT, Sabatini BL. Supraresolution imaging in brain slices using stimulated-emission depletion two-photon laser scanning microscopy. Neuron 2009, 63: 429–437.

[35] Urban NT, Willig KI, Hell SW, Nagerl UV. STED nanoscopy of actin dynamics in synapses deep inside living brain slices. Biophys J 2011, 101: 1277–1284.

[36] Berning S, Willig KI, Sfeffens H, Dibaj P, Hell SW. Nanoscopy in a living mouse brain. Science 2012, 335: 551.

[37] Liu KS, Siebert M, Mertel S, Knoche E, Wegener S, Wichmann C, *et al.* RIM-binding protein, a central part of the active zone, is essential for neurotransmitter release. Science 2011, 334: 1565–1569.

[38] Hua Y, Sinha R, Thiel CS, Schmidt R, Huve J, Martens H, *et al.* A readily retrievable pool of synaptic vesicles. Nat Neurosci 2011, 14: 833–839.

[39] Denker A, Krohnert K, Buckers J, Neher E, Rizzoli SO. The reserve pool of synaptic vesicles acts as a buffer for proteins involved

in synaptic vesicle recycling. Proc Natl Acad Sci U S A 2011, 108: 17183–17188.

[40] Huang B, Bates M, Zhuang X. Super-resolution fluorescence microscopy. Annu Rev Biochem 2009, 78: 993–1016.

[41] Xu K, Babcock HP, Zhuang X. Dual-objective STORM reveals three-dimensional filament organization in the actin cytoskeleton. Nat Methods 2012, 9: 185–188.

[42] Bates M, Huang B, Dempsey GT, Zhuang X. Multicolor super-resolution imaging with photo-switchable fluorescent probes. Science 2007, 317: 1749–1753.

[43] Shroff H, Galbraith CG, Galbraith JA, White H, Gillette J, Olenych S, *et al*. Dual-color superresolution imaging of genetically expressed probes within individual adhesion complexes. Proc Natl Acad Sci U S A 2007, 104: 20308–20313.

[44] Bates M, Dempsey GT, Chen KH, Zhuang X. Multicolor super-resolution fluorescence imaging via multi-parameter fluorophore detection. Chemphyschem 2012, 13: 99–107.

[45] Westphal V, Rizzoli SO, Lauterbach MA, Kamin D, Jahn R, Hell SW. Video-rate far-field optical nanoscopy dissects synaptic vesicle movement. Science 2008, 320: 246–249.

[46] Jones SA, Shim SH, He J, Zhuang X. Fast, three-dimensional super-resolution imaging of live cells. Nat Methods 2011, 8: 499–508.

[47] Dani A, Huang B, Bergan J, Dulac C, Zhuang X. Superresolution imaging of chemical synapses in the brain. Neuron 2010, 68: 843–856.

[48] Frost NA, Shroff H, Kong H, Betzig E, Blanpied TA. Single-molecule discrimination of discrete perisynaptic and distributed sites of actin filament assembly within dendritic spines. Neuron 2010, 67: 86–99.

[49] Tardin C, Cognet L, Bats C, Lounis B, Choquet D. Direct imaging of lateral movements of AMPA receptors inside synapses. EMBO J 2003, 22: 4656–4665.

[50] Heine M, Groc L, Frischknecht R, Beique JC, Lounis B, Rumbaugh G, *et al.* Surface mobility of postsynaptic AMPARs tunes synaptic transmission. Science 2008, 320: 201–205.

[51] Kerr JM, Blanpied TA. Subsynaptic AMPA receptor distribution is acutely regulated by actin-driven reorganization of the postsynaptic density. J Neurosci 2012, 32: 658–673.

[52] Derosier DJ, Klug A. Reconstruction of three dimensional structures from electron micrographs. Nature 1968, 217: 130–134.

[53] Ruiz T, Erk I, Lepault J. Electron cryo-microscopy of vitrified biological specimens: towards high spatial and temporal resolution. Biol Cell 1994, 80: 203–210.

[54] Adrian M, Dubochet J, Lepault J, McDowall AW. Cryo-electron microscopy of viruses. Nature 1984, 308: 32–36.

[55] Erk I, Michel M, Lepault J. Electron cryo-microscopy of vitrified bulk biological specimens: ideal and real structures of water-lipid phases. J Microsc 1996, 182: 15–23.

[56] Kirschning E, Rutter G, Hohenberg H. High-pressure freezing and freeze-substitution of native rat brain: Suitability for preservation and immunoelectron microscopic localization of myelin glycolipids. J Neurosci Res 1998, 53: 465–474.

[57] Vanhecke D, Asano S, Kochovski Z, Fernandez-Busnadiego R, Schrod N, Baumeister W, *et al.* Cryo-electron tomography: methodology, developments and biological applications. J Microsc 2011, 242: 221–227.

[58] Zuber B, Nikonenko I, Klauser P, Muller D, Dubochet J. The mammalian central nervous synaptic cleft contains a high density of periodically organized complexes. Proc Natl Acad Sci U S A 2005, 102: 19192–19197.

[59] Chen X, Winters C, Azzam R, Li X, Galbraith JA, Leapman RD, *et al.* Organization of the core structure of the postsynaptic density. Proc Natl Acad Sci U S A 2008, 105: 4453–4458.

[60] Chen X, Nelson CD, Li X, Winters CA, Azzam R, Sousa AA, *et al.* PSD-95 is required to sustain the molecular organization of the postsynaptic density. J Neurosci 2011, 31: 6329–6338.

[61] Liu J, Taylor DW, Krementsova EB, Trybus KM, Taylor KA. Three-dimensional structure of the myosin V inhibited state by cryoelectron tomography. Nature 2006, 442: 208–211.

[62] Grunewald K, Desai P, Winkler DC, Heymann JB, Belnap DM, Baumeister W, *et al.* Three-dimensional structure of herpes simplex virus from cryo-electron tomography. Science 2003, 302: 1396–1398.

[63] Milne JL, Subramaniam S. Cryo-electron tomography of bacteria: progress, challenges and future prospects. Nat Rev Microbiol 2009, 7: 666–675.

[64] Nicastro D, Frangakis AS, Typke D, Baumeister W. Cryo-electron tomography of neurospora mitochondria. J Struct Biol 2000, 129: 48–56.

[65] Fernandez-Busnadiego R, Schrod N, Kochovski Z, Asano S, Vanhecke D, Baumeister W, *et al.* Insights into the molecular organization of the neuron by cryo-electron tomography. J Electron Microsc (Tokyo) 2011, 60 (Suppl 1): S137–148.

[66] Fernandez-Busnadiego R, Zuber B, Maurer UE, Cyrklaff M, Baumeister W, Lucic V. Quantitative analysis of the native presynaptic cytomatrix by cryoelectron tomography. J Cell Biol 2010, 188: 145–156.

[67] Beck M, Lucic V, Forster F, Baumeister W, Medalia O. Snapshots of nuclear pore complexes in action captured by cryo-electron tomography. Nature 2007, 449: 611–615.

[68] Alber F, Dokudovskaya S, Veenhoff LM, Zhang W, Kipper J, Devos D, *et al.* Determining the architectures of macromolecular assemblies. Nature 2007, 450: 683–694.

[69] Lucic V, Kossel AH, Yang T, Bonhoeffer T, Baumeister W, Sartori A. Multiscale imaging of neurons grown in culture: from light microscopy to cryo-electron tomography. J Struct Biol 2007, 160:

146–156.

[70] Lucic V, Yang T, Schweikert G, Forster F, Baumeister W. Morphological characterization of molecular complexes present in the synaptic cleft. Structure 2005, 13: 423–434.

[71] Sartori A, Gatz R, Beck F, Rigort A, Baumeister W, Plitzko JM. Correlative microscopy: bridging the gap between fluorescence light microscopy and cryo-electron tomography. J Struct Biol 2007, 160: 135–145.

[72] Landis DM, Hall AK, Weinstein LA, Reese TS. The Organization of cytoplasm at the presynaptic active zone of a central nervous-system synapse. Neuron 1988, 1: 201–209.

[73] Siksou L, Rostaing P, Lechaire JP, Boudier T, Ohtsuka T, Fejtova A, *et al.* Three-dimensional architecture of presynaptic terminal cytomatrix. J Neurosci 2007, 27: 6868–6877.

[74] Dalva MB, McClelland AC, Kayser MS. Cell adhesion molecules: signalling functions at the synapse. Nat Rev Neurosci 2007, 8: 206–220.

[75] Gerrow K, El-Husseini A. Cell adhesion molecules at the synapse. Front Biosci 2006, 11: 2400–2419.

[76] Kennedy MB. Signal-processing machines at the postsynaptic density. Science 2000, 290: 750–754.

[77] Takumi Y, Ramirez-Leon V, Laake P, Rinvik E, Ottersen OP. Different modes of expression of AMPA and NMDA receptors in hippocampal synapses. Nat Neurosci 1999, 2: 618–624.

[78] Kharazia VN, Weinberg RJ. Tangential synaptic distribution of NMDA and AMPA receptors in rat neocortex. Neurosci Lett 1997, 238: 41–44.

[79] Ji N, Shroff H, Zhong H, Betzig E. Advances in the speed and resolution of light microscopy. Curr Opin Neurobiol 2008, 18: 605–616.

[80] Freitag B, Bischoff M, Mueller H, Hartel P, von Harrach HS. Subnanometer resolution in field-free imaging using a Titan80-300 with Lorentz lens and image Cs-corrector at 300kV acceleration voltage. Microsc Microanal 2009, 15: 184–185.

[81] Fukuda Y, Nagayama K. Zernike phase contrast cryo-electron tomography of whole mounted frozen cells. J Struct Biol 2012, 177: 484–489.

[82] Murata K, Liu X, Danev R, Jakana J, Schmid MF, King J, *et al.* Zernike phase contrast cryo-electron microscopy and tomography for structure determination at nanometer and subnanometer resolutions. Structure 2010, 18: 903–912.

[83] Jin L, Milazzo AC, Kleinfelder S, Li SD, Leblanc P, Duttweiler F, *et al.* Applications of direct detection device in transmission electron microscopy. J Struct Biol 2008, 161: 352–358.

[84] Zanetti G, Riches JD, Fuller SD, Briggs JA. Contrast transfer function correction applied to cryo-electron tomography and subtomogram averaging. J Struct Biol 2009, 168: 305–312.

[85] Beck M, Malmstrom JA, Lange V, Schmidt A, Deutsch EW, Aebersold R. Visual proteomics of the human pathogen Leptospira interrogans. Nat Methods 2009, 6: 817–823.

[86] Shu X, Lev-Ram V, Deerinck TJ, Qi Y, Ramko EB, Davidson MW, *et al.* A genetically encoded tag for correlated light and electron microscopy of intact cells, tissues, and organisms. PLoS Biol 2011, 9: e1001041.